Imaging the evolution of visual specializations in fungus gnats

Gavin J. Taylor[1]*, Stephen A. Hall[2], Johan A. Gren[3], and Emily Baird[1]*
[1]Department of Biology, Lund University, Sweden
[2]Division of Solid Mechanics, Lund University, Sweden
[3]Department of Geology, Lund University, Sweden
*Corresponding authors: gavin.taylor.01@gmail.com and emily.baird@biol.lu.se

Keywords:
Eye evolution, sensory adaptation, visual specialization, optical analysis, visual simulation, insect eyes, microCT, fungus gnat, amber, museum collections

Abstract:
Unraveling how behavioral, environmental, and phylogenetic factors shape the evolution of eyes is difficult because existing methods for analyzing visual systems require specific preservation protocols that limit the use of historical specimens and fossils. To broaden the range of specimens that can be utilized for studies on eye evolution, especially those from museum collections, we developed a novel analysis technique that uses x-ray microtomography to create optical models that enable us to quantify the vision of arthropod compound eyes. We demonstrate our methodology with an investigation into the visual specializations that fungus gnats have evolved over the last 30 million years and demonstrate its flexibility by using specimens in three different states of preservation. Our analyses show that gnats from different forest types and time periods have distinct visual specializations, confirming that this method provides a new approach to study the sensory evolution of compound eyes.

Introduction:
Vision provides essential information to meet the sensory demands of many animals and is important for orchestrating both movement through, and interactions with, their environment[1]. To meet the sensory demands of visually-guided behavior, animal eyes typically contain specialized regions of high resolution and/or sensitivity that are optimized for acquiring information to guide specific behavioral tasks. Another, less well understood factor affecting visual adaptations is the environment itself because specific features, such as the illumination and presence of a clear horizon may vary dramatically: consider, for example, the difference between a bright open meadow and a dim cluttered rainforest[3]. To acquire the visual information necessary for guiding behavior in these different environments, animal eyes are also likely to have habitat-specific visual adaptations. Understanding these specializations is crucial for understanding the sensory world of animals and the role that the visual system has in defining the range and type of habitats an animal can survive in.

The corneal structure of the arthropod compound eye is commonly used to identify visual specializations from the external size and distribution of the corneal facets, which are often preserved naturally on samples in taxonomic collections. The diverse range of arthropod specimens existing in museum collections thus provides an ideal resource for the comparisons needed to study whether and how eyes evolve habitat specific adaptations. However, current methods for analyzing compound eyes are unsuitable for such investigations because i) many methods require fresh tissue and can only be performed on readily available extant species[4], and ii) most methods provide only a 2D representation of the compound eye and thus limit our ability to understand how it viewed its 3D environment[5]. To overcome these limitations, we developed a method to quantify and recreate the visual world of naturally preserved arthropod eyes using x-ray microtomography – a popular tool for morphological and structural analysis in many fields – as the basis for modelling the optical function of insect eyes[6]. Arthropod compound eyes are composed of many facets, also known as ommatidial units, that comprise a corneal lens, a crystalline cone and an underlying group of photoreceptors[1]. Using the shape of the cornea in 3D corneal models, we can calculate information about the local resolution and relative sensitivity across an eye, as well as the extent of its visual field. The measured data can be displayed in world-based coordinates, which facilitates direct comparisons between eyes with different morphologies or sizes. Because our method is non-destructive and is based only on the corneal structure, it is suitable to perform on fossils or samples that are preserved in collections and enables investigations into the factors that drive and shape the visual evolution of compound eyes.

We demonstrate our analysis technique by examining the visual specializations of fungus gnats from different habitats and different evolutionary time periods. Astonishingly, while these tiny insects are amongst the smallest flies, they are capable of inhabiting some of the most visually complex habitats on earth[7]. Species of fungus gnats inhabit a broad range of forest types, from the arctic to the tropics, and their frequent occurrence in amber shows they have thrived for at least 50 million years[8]. We focus our study on females from three species of the cosmopolitan Orfeliini tribe, 1) an ancient species (Orfeliini sp.; Fig. S1) from the tropical rainforests of Scandinavia ~30 million years ago, 2) an extant species from the tropical rainforests of Africa (*Rutylapa* sp.), and 3) an extant species from the temperate forests of modern Scandinavia (*Neoplatyura modesta*). While both Scandinavian gnats are from a similar geographic location, they represent species from different habitat types as forests in the Baltic region have thinned substantially in the last 30 million years[9]. For the continued evolutionary success of these diminutive Dipterans, each species must have remained capable of acquiring the visual information necessary to control flight through its particular habitat. Yet the eye specializations evolved for one habitat may not be optimal for other visual environments. We hypothesized that the visual properties of the two tropical gnat species would be the most similar, despite the distance between their geographic and temporal distributions. Specifically, given that tropical forests are relatively dark due to their dense canopies, we expected that tropical gnats could have specializations that improve their optical sensitivity and that these may not be possessed by gnats that inhabit brighter temperate forests. The aim of this study is to determine whether the miniature eyes of gnats evolved *different* visual specializations depending on their specific visual habitat and if so, what were they?

Results

Our novel analysis technique uses laboratory x-ray microtomography to image the 3D structure of the heads of gnats (Fig. 1Ai, ii). We then calculate the visual properties of the eyes from the structure, shape and size of the individual corneal lenses (Fig. 1Aiii-v). The corneal lenses provide details about the limits of resolution and sensitivity in a particular region of the eye, as well as enabling us to determine the full extent of the visual field. The diameter (D) of the lenses indicates the amount of light that is focused onto the underlying photoreceptors. Larger lenses capture additional light in proportion to the square of their diameter and increase optical sensitivity considerably (other factors influencing sensitivity include the receptor dimensions and its optical acceptance angle)[2]. Each lens also focuses light from a specific region of space, or viewing direction, that is centered about its optical axis. The smaller the angle between the optical axes of adjacent lenses (the inter-ommatidial angle, $\Delta\Phi$), the greater the visual resolution in that part of the visual field[2]. By analyzing the distribution of lenses across the compound eye in 3D, we can determine the optical axis each corneal lens and the entire eye's field of view (Fig. 1Avi, vii), as well as the associated lens diameter and inter-ommatidial angle (Fig. 1Aviii). Our analysis procedure is described in detail in the 'Online methods' section.

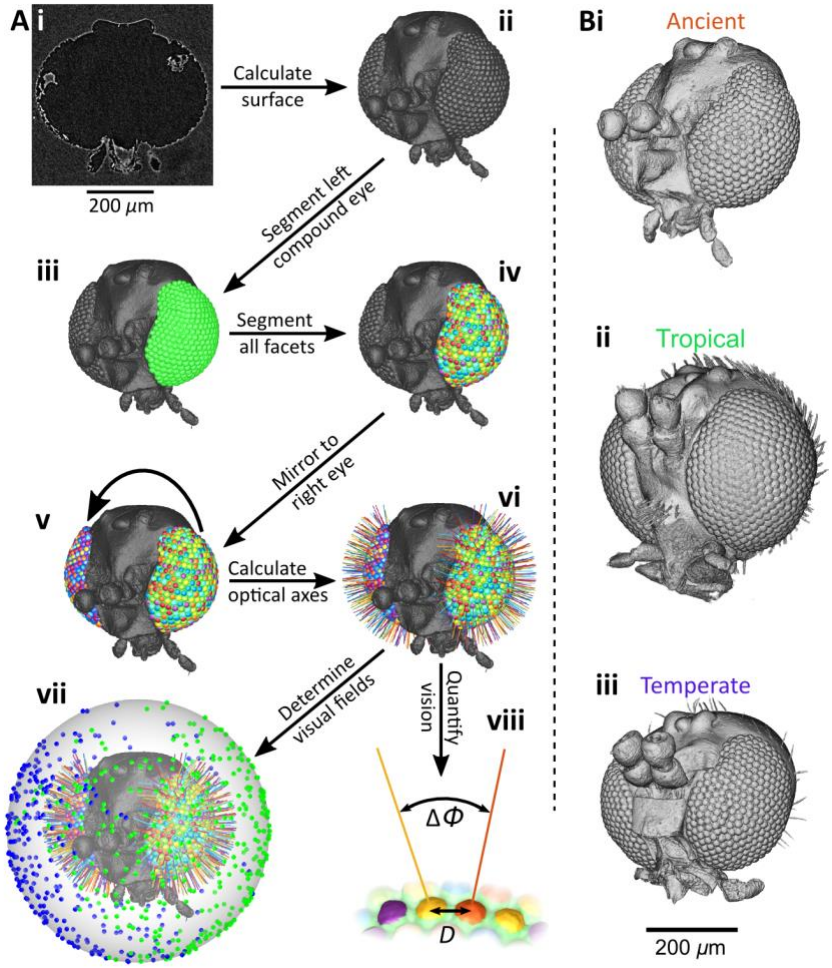

Figure 1: (**A**) Workflow to quantify the visual parameters of an insect eye from x-ray microtomography. (**i**) Virtual section through a reconstructed volume showing the head of an Eocene fungus gnat from an amber endocast. (**ii**) The reconstructed exterior surface of the gnat's head. (**iii**) The segmented left compound eye, and (**iv**) all of its segmented corneal lenses. (**v**) The left eye mirrored to the right-hand side of the head, and (**vi**) the calculated optical axis of all lens surfaces. (**vii**) The optical axes are projected onto a sphere to determine their viewing directions and visual fields (green – left eye, blue – right eye). (**viii**) Visual parameters can be calculated across the eye: lens diameter (*D*) and inter-ommatidial angle (ΔΦ). (**B**) Volume renderings of each gnat imaged for this study. (**i**) Endocast of Orfeliini sp. in Eocene Baltic amber; (**ii**) alcohol-preserved head of *Rutylapa* sp.; and (**iii**) dried head of *N. modesta*. The scale bar underneath Biii applies to the renderings of all heads.

To investigate whether and how the visual systems of fungus gnats have changed both across habitat type and across time, we applied our technique to three species (Orfeliini sp. – ancient, tropical, Fig. 1Bi; *Rutylapa* sp. – extant, tropical, Fig. 1Bii; *N. modesta* – extant, temperate, Fig. 1Biii). The exterior corneal surfaces reconstructed from x-ray microtomography showed that, superficially, the ancient gnat appears most similar to the extant temperate species (Fig. 1B). While the head and eye size of the ancient gnat was between those of the two extant gnats (Table S1), the ancient gnat had both larger lens diameters (Fig. 2D) and inter-ommatidial angles (Fig. 2E), and also a larger field of view than either extant species (Table S1). Interestingly, all species have a part of the visual field viewed by both eyes – a binocular overlap – and this is directed ventrally and frontally (Fig. 2A-C). Despite the gnats' small eyes, it is evident that they also possess regional visual specializations. For example, the inter-ommatidial angles vary across the visual field of all gnats. The lowest inter-ommatidial angles (indicating higher resolution) are directed laterally and view their monocular visual field (Fig 2A-C:ii). Furthermore, a ventral to dorsal reduction in lens diameter is visible across the visual fields of both tropical specimens (Fig. 2A,B:i), but this is not apparent on the temperate gnat's eye (Fig. 2C:i). A simulation of the spatial sampling of both eyes on each gnat

indicates that all three should obtain coarse, but distinct, spatial information from the features in a forest scene (Fig. 3).

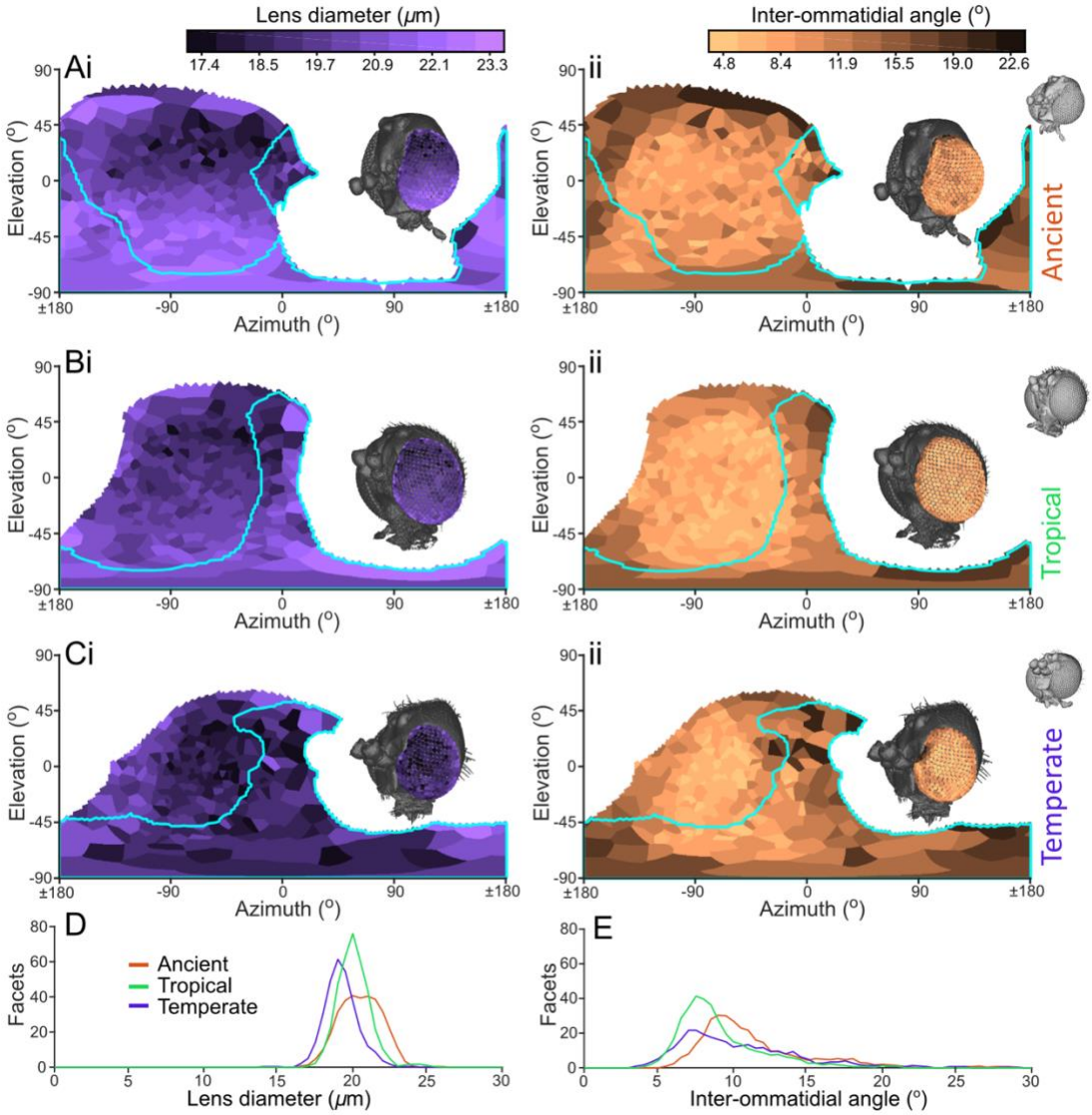

Figure 2: Visual quality of fungus gnat eyes for (**A**) the ancient gnat, (**B**) the extant tropical gnat, and (**C**) the extant temperate gnat, with maps of (**i**) the lens diameter and (**ii**) the inter-ommatidial angle, as they are projected onto the visual world. These parameters are also shown directly on the corneal lenses in the inset of each panel. Note that a lower angle indicates higher resolution vision. Each gnat is facing towards 0° azimuth, and the cyan lines indicate the limit of binocular field of view. The frequency distribution of lens diameter (*D*) and inter-ommatidial angle (ΔΦ), for each individual are shown in (**D**) and (**E**), respectively.

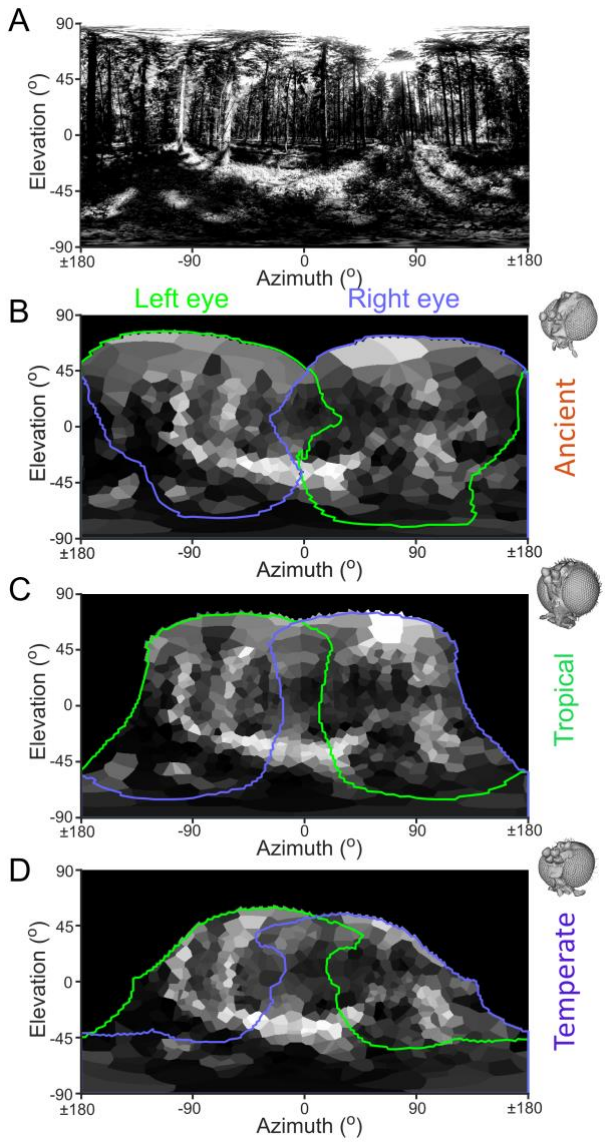

Figure 3: A forest viewed through the eyes of different gnat species. (**A**) An equirectangular projection of a 360° panoramic image of a European forest in summer (image: istock.com/Bestgreenscreen). (**B**) Simulated view of the scene with data quantified from the eyes of the ancient gnat, and likewise, from the eyes of the extant tropical (**C**) and the temperate (**D**) gnats. Each gnat is facing towards 0° azimuth and the green and mauve lines denote the limits of the visual field for the left and right eyes respectively. The simulation accounted for the variation in visual resolution (but *not* any spatial variation in optical sensitivity) across each eye's field of view.

Discussion

Vision is essential for guiding many animal behaviors, but we know little about the intrinsic and extrinsic factors driving the evolution of visual systems and their adaptation to specific visual environments. This knowledge gap is partly due to the limitations of current methodologies for quantifying eye specializations, which can only be applied to freshly preserved tissue, thereby preventing investigations of rare, naturally preserved, or ancient specimens[4]. To overcome this, we have developed a new method for exploring the visual world of arthropods using non-destructive x-ray microtomographic methods (Fig. 1Ai) that can be applied equally well to fresh, dried, or even fossilized compound eyes. We demonstrated this method by quantifying the vision of fungus gnats' tiny eyes.

While not readily apparent from their external morphology (Fig. 1B), our analysis of gnat vision reveals that different species do indeed appear to have evolved visual specializations that would optimize their compound eyes for their specific habitats. In particular, we identified two visual specializations *common* to

all three of the Orfeliini species investigated. The first is that their highest resolution vision is directed laterally (Fig. 2A-C:i). This is in contrast to larger Dipterans (including *Drosophila*), whose highest resolution is directed frontally[10-12]. The second specialization common to the species investigated here is that they have a large binocular visual field that is primarily directed ventrally and somewhat frontally (Fig. 3). Interestingly, the extent of binocular visual field in larger female flying insects is typically smaller and approximately ventrally-to-dorsally symmetric[13-15]. We propose that ventral binocularity is a previously unconsidered adaption for small, forest-dwelling insects that could allow them to improve sensitivity by integrating the noisy signal in shadowed objects on the ground between both eyes. In addition to revealing commonalities in the visual systems of the different fungus gnats, our method also revealed that they have distinct *differences*, which appear to be habitat-specific specializations. We find that both the extant and ancient tropical gnat species have a larger, more dorsally-directed total visual field than the temperate gnat (Fig. 3). Another difference is that while the lens diameters remain relatively constant across the temperate gnat's eyes, the lens diameters in the tropical gnats have a clear negative relationship to elevation, as their ventral lenses are larger than those facing dorsally (Fig. 2A,B:i). These larger ventral lenses are a regional visual specialization that would improve the relative sensitivity of the ommatidia viewing the forest floor. An analogous increase in eye 'regionalization' is also found among extant damselfly species that live in dark or visually complex habitats[16]. In combination with the ventral binocular overlap, this ventral region of high sensitivity in the tropical gnats suggests that the ground is an important source of visual information for these insects. Taken together, our findings support our initial hypothesis that the tropical gnat species do indeed have specific specializations to increase optical sensitivity compared to their temperate relatives.

Our results demonstrate that the proposed analysis method can be used to identify specific visual specializations present in species from different times and environments and will enable investigations into the visual systems of rare or extinct species in various states of preservation. We acknowledge that the strength of our conclusions are limited by the sample size, but these preliminary investigations provide justification for larger, more detailed studies with samples from a broader range of species. A distinct advantage of our method is that it facilitates direct comparisons of vision between species. Unlike existing approaches, the method enables the visual properties of each insect to be presented in a common, world-based coordinate frame, even if there are substantial differences between the visual morphology or size of the eyes. Additionally, the ability of this technique to simulate vision through an insect's eyes provides insights into how it views a particular scene (Fig. 3), which is a valuable tool for developing hypotheses about the function of specific visual adaptations, which can then be directly tested with behavioral experiments. For instance, despite being weak fliers, fungus gnats are effective pollinators[17]. Is it possible that the eyes of tropical species allow them to find flowers more easily in a rainforest than the eyes of temperate species would? Knowledge of a gnat's visual capabilities and simulating its vision undoubtedly provide a crucial starting point for designing behavioral assays to conclusively answer such a question.

The cuticular corneas of insect eyes can remain exceptionally preserved in amber dating back to the Early Cretaceous[18] and we expect that there are many further opportunities to use our methodology to study the circumstances through which specific visual traits evolved in other taxa. For example, prominent acute zones with regions of flattened and enlarged lenses have evolved to accompany pursuit behavior in many insect species. Identification of such regional specializations in the fossil record could, for instance, be used to investigate the evolutionary origins of pursuit mating strategies in male bees[19]. Fine retinal structures can be identified in our alcohol-preserved sample (Fig. S2) and are also likely to be visible in images of well-preserved amber inclusions[21] which could provide additional insights into the visual systems of ancient insects. X-ray microtomography has been used to describe the morphology of insect inclusions for taxonomic purposes[22,23] and data obtained for systematics could also be used to describe a specimens vision. Applying our methodology to the substantial range of dried specimens collected over the last two centuries[24] would also facilitate investigations into the influence of recent anthropogenic disruptions on the evolution of invertebrate visual systems. For example, our methodology could be used to examine whether the increase in light pollution over the last century has placed selective pressure on the eyes of nocturnal urban insects [25,26]. Testing these, and many other, hypotheses related to the factors driving visual evolution will be possible by applying this technique to analyze the well-preserved compound eyes of the arthropod specimens available in museum collections.

Acknowledgments
We would like to thank Rune Bygebjerg from the Department of Biology at Lund University and Gier Søli from the Natural History Museum at the University of Oslo for supplying the extant samples used in this study, and Vladimir Blagoderov from the London Natural History Museum for assisting with the identification of the amber embedded specimen. Additionally, we are most indebted to Viktor Håkansson for his meticulous segmentation of the data. Gavin Taylor is thankful to have received a stipend from Carl Tryggers Stiftelse (CTS15:38) and an endowment from the Royal Physiographic Society of Lund, while Emily Baird gratefully acknowledges financial support from the Air Force Office of Scientific Research (FA8655-12-1-2136), the Swedish Research Council (2014-4762), and the Lund University Natural Sciences Faculty.

Author Contributions
Conceptualization, G.J.T., J.A.G., and E.B.; Methodology, G.J.T, J.A.G., S.A.H., and E.B.; Software, G.J.T.; Investigation, G.J.T. and E.B.; Formal Analysis, G.J.T. and S.A.H.; Writing – Original Draft, G.J.T. and E.B.; Writing – Review & Editing, G.J.T., J.A.G., S.A.H., and E.B.; Visualization, G.J.T.; Funding Acquisition, G.J.T. and E.B.; Resources, J.A.G.; Supervision, G.J.T. and E.B.

Competing Interests
The authors declare no competing interests.

Online methods
Animals
Each of the three fungus gnat species were preserved in a different way – dried, in alcohol, or as an amber endocast (Table S1). We only selected females for our analysis to minimize the effect of sexual dimorphism, as the males of some Dipteran species are known to have evolved visual specializations related to pursuit flights during courtship[27]. The Entomology Collection at the Department of Biology, Lund University provided dried and pinned samples of *Neoplatyura modesta*, the Natural History Museum at the University of Oslo provided samples of *Rutylapa* sp. preserved in ethanol, while the Department of Geology at Lund University provided a piece of amber containing inclusions of Orfeliini sp. (Fig. S1). The smallest individuals with intact eyes (as observed with a light microscope) from the samples available for each species were chosen for microtomographic analysis, from which we found they varied in head width by approximately 20% (Table S1).

Microtomography
X-ray microtomography was performed on the head of each sample using a Zeiss XRM520 at the 4D Imaging Lab at Lund University. For each data set, x-ray projections were obtained over 360° (for specific scanning parameters see Table S2) and reconstructed into 3D volumes with 1μm isotropic resolution. Due to their different preservation states, each sample was mounted in the tomograph using a different method, as outlined below.

- The pin of the dried sample was clamped in a pin-vice and mounted directly in the tomograph and was oriented such the pin did not occlude the projection of the gnat head on the detector.
- The alcohol-preserved sample was placed at the bottom of a 0.5 mL microcentrifuge tube (Eppendorf) and partially covered with a small amount of 70% ethanol (the surface tension of the liquid held the gnat in place). A ball of Parafilm was then used to fill the remaining volume of the tube and prevent evaporation of the ethanol. The original microcentrifuge tube was placed partially within a larger 2 mL tube and secured with Parafilm, and the later was clamped in a pin-vice and mounted in the tomograph.
- The amber block was hot-glued to a 'drawing pin' that was clamped in a pin-vice and mounted in the tomograph. A lower resolution scan was initially conducted on the block to identify the location of several inclusions, with the head of one selected for the 1μm resolution scans.

General analysis procedure
Performing x-ray microtomography on the head of gnats allowed the lenses of the compound eye to be identified (Fig. 1Ai) and digital representation of the entire head surface to be computed (Fig. 1Aii) in Amira (FEI). The border of the left eye (Fig. 1Aiii) and each of its lenses (Fig. 1Aiv) were then manually

labeled by selecting paths across the surface. This isolated the surface of every individual lens in the left eye. The right eye was represented by mirroring the lens surfaces of the left eye (Fig. 1Av). For additional information on these steps, see the 'Detailed surface analysis procedure' section below.

The optical axis of each lens (Fig.1Avi) and its viewing direction relative to the head (Fig.1Avii) were calculated from the surfaces after importing them into Matlab (Mathworks). The limits of the visual field of each eye were calculated from the optical axes of their outermost lenses. The complete visual field and binocular overlap was determined by combining the limits of both eyes (Fig. 1Avii). Lens diameters were calculated by finding the average distances between the center of each facet and its neighbors (Fig. 1Aviii) and inter-ommatidial angles were calculated by finding the average angle between the optical axis of a facet and its neighbors (Fig. 1Aviii)[2]. Diagrams of how lens diameter and inter-ommatidial angle vary over the visual field were generated from the visual axes and properties calculated for each gnat. A voronoi diagram was drawn around the visual axes of each eye, and the cells were colored according to the local lens diameter (Fig. 2A-C:i) or inter-ommatidial angle (Fig. 2A-C:ii), which could also be depicted by coloring the individual lenses of the compound eye (Fig. 2A-C insets). A simulation of how each gnat may have viewed a forest scene was generated from an arbitrarily chosen panoramic forest image. We assumed that each lens accepted light over an angle equal to its inter-ommatidial angle, and then colored the voronoi cells based on the weighted average of the intensity value of the pixels that lay within this angular range (Fig. 3). For additional information on these steps, see the 'Detailed computational analysis procedure' section below.

Detailed surface analysis procedure

Each image stack from microtomography was imported into Amira (v6.2, FEI), within which an interactive workflow was developed that allowed us to create a surface defining the head of the scanned insect, and then to delineate the border of the left eye plus each corneal lens on it. After labeling the lenses, these data were mirrored to the right eye, and the surface data and mirror transform were then exported to Matlab for further computational analysis (see the following section). In the following descriptions, windows within the Amira console are indicated in *italics*, Editor windows (accessible from the *Properties View* of a module) are indicated by <u>underlining</u>, and further modules, tools, and options are indicated in 'parenthesis'.

The head surface was created by first labelling the voxels within the head volume, and then fitting a surface around their border, as described in the following. The 'Threshold' tool in the *Segmentation View* was used to select and label the voxels that were part of a gnat (which were lower intensity than the surrounding material for the amber-embedded specimen, but higher in the other two cases). The '3D Lasso' tool was then used to select and remove excess labeled material, such that only the fungus gnat's head capsule remained labeled. Following this, a surface was created around the labels using the 'Generate Surface' (a 'smoothing extent' of 2 was used when generating the surface) and 'View Surface' modules in the *Project View*. Sometimes the surface created for the eyes appeared to be poorly formed, particularly for the amber-embedded and alcohol-preserved samples. In the former case, this was because decayed material from the gnat coated the inside of the endocast, and often had higher absorption than the amber. In the alcohol-preserved case, it was because of relatively low absorption contrast between the cuticle and the alcohol. In both cases, the 'Brush' tool was used to manually correct the label field of 2D slices in the *Segmentation Editor*, to ensure that individual lens surfaces of the left eye appeared smooth in the generated surface and, additionally, that the surface of the eye was closed, with no gaps present between lenses. The scan of the dried gnat had high contrast between the cuticle and air and the initial surface that was generated did not require such corrections.

After completing any required corrections, a final surface was created and a 'Create Surface Geodesic Path' module was attached to it (all remaining steps are performed in the *Project View*). In the <u>Surface Path Editor</u>, the connector was set to 'dijkstra', and the control points to 'vertex'. The <u>Surface Path Editor</u> allows points to be selected around the border of the left compound eye, which were linked by paths taking the shortest route across the surface between sequential points. To isolate this area from the remainder of the surface, after closing the path around the eye, the 'Patchify Surface' was selected. The <u>Surface Editor</u> was then used to selectively display only the compound eye patch, after which the 'Extract Surface' module was used to create a new surface only including the compound eye. A second 'Create

Surface Geodesic Path' module was then attached to the isolated corneal surface and paths were traced in a circle around the base of every lens on the compound eye. Approximately 60 control points were placed per lens and closing a path upon completion allowed a new path to be started for the next lens. Note that each fungus gnat lens has a dome shaped cornea; many other insects have flatter, hexagonal lenses and placing a control point at each of the six corner points of a lens would probably be sufficient in such cases. The right eyes of gnats were not individually segmented, but we counted the number of lenses by using another geodesic path to place control points at the center of each facet. This indicated that the gnat eyes were approximately symmetrical, with at most a 2.4% difference in facet number between the eyes (Table S1).

Each head surface was then aligned using the Transform Editor, by positioning and aligning it such that it faced forwards in the default XY image in the *Project view*. The head was aligned in its frontal (yaw) and axial (roll) planes based on its symmetry. The pitch (sagittal plane) of the head could not be aligned by symmetry, but was positioned such that each head appeared to have a similar, forwards facing, orientation (Fig. 2A-C). While the orientation of the head may vary during flight this provides a consistent reference frame between insects. After aligning the head, the resulting rigid transformation matrix was copied to both the isolated eye surface and the paths around each facet. While the right eye was not separately labeled, we determined the transformation required to mirror the labelled left eye such that it was aligned with the position of the right eye. To mirror the left eye, we used the 'Scan surface to volume' module on the left eye surface to create a volume in which the voxels corresponding to the surface were labeled. The 'Resample transformed image' module was then applied to this volume, which created a second volume, the axes of which were orthogonal to the world coordinate frame. This volume could then be mirrored around the sagittal plane of the head by using the 'Flip X' button in the Crop Editor, and a 'Volume rendering' module was used to visualize the position of the mirrored eye. Finally, the Transform Editor was used to adjust the alignment of the mirrored right eye such that it matched the actual right eye on the surface of the head as closely as possible.

After completing the above-described processing workflow in Amira (which typically required several hours per dataset), it was necessary to export data for use in Matlab. Both the head surface and eye surface were exported as 'stl' files in little endian format. The paths surrounding each facet were exported as 'Amira lineset' files in asci format. To facilitate importing paths into Matlab, it was necessary to split the lineset file into two parts using a text editing program. Each file contains data under two headings; @1 is a list of indices indicating the vertices to use for each control point in an individual path (-1 indicates that start of a new path), @2 is a list of 3D vertices coordinates referenced by the indices. It is necessary to copy the indices and vertices into individual text files. Finally, the 4x4 transform matrices for the head and the right eye were recorded by using the 'GetTransform' command in the *TCL Console*, and the 'Max index' and the 'Min coord' values of the right eye volume were recorded from Crop Editor.

Upon acceptance of this manuscript: We will submit the original volumes and head surfaces from each sample to the MorphoSource depository and include their DOIs in the manuscript. We will also submit an example Amira project showing the result of the complete workflow described above as Supplementary Material.

Detail computational analysis procedure

The data exported by Amira was imported into Matlab and analyzed using a series of custom written scripts to quantify the visual properties of gnat eyes and perform a visual simulation. The analysis procedure involves applying the rigid transformations to the imported surfaces and identifying the lens surfaces from the path points. The corneal optical axis from each lens was calculated, from which the eye's visual parameters and fields of view were quantified. Various plotting options were implemented for the data, including performing a visual simulation of the insect's perspective of a scene. This analysis was mostly automated, and here we describe the analysis steps performed by the script. Variable names that the user may wish to modify are indicated in 'parenthesis', and influence data importing and various display options as outlined in the initial 'Configuration' section of the supplemental 'AnalyseCorneaMain.m' file.

Data were initially imported into Matlab based on the user specified files in the initial portion of the 'Configuration' section. The appropriate transformations were applied to the surfaces such that they were represented in the same orientation as seen in Amira. The paths were initially formatted as a single list of points, but we separated this into an individual list of vertices for each lens' border. After this, the coordinates on the eye surface enclosed by each border path were selected as the corneal surface for that facet. The geometric center point of the cornea of each lens was determined, and then the normal vector of the corneal surface was calculated from this point. This calculation involved fitting a second order polynomial surface to the corneal surface vertices, and calculating the normal direction from the derivative at the central point[28]. The normal vector was taken to indicate the optical axis of the lens. The same procedure was performed for the mirrored right eye.

The neighbors of each lens were determined based on the shortest distances between its center and those of each other lens (each lens was linked to six neighbors, unless it was on the border of the eye). Having established the neighbors of each lens, the inter-ommatidial angle ($\Delta\Phi$) of a given lens was calculated as the average angle between its optical axis and those of its neighbors and the lens diameter (D) was calculated as the average distance from its center point to those of its neighbors. Additionally, the eye parameter (P), was calculated by multiplying each lens' inter-ommatidial angle by its diameter[29]. It was not possible for us to calculate the acceptance angle over which individual lenses absorbed light, hence we assumed that this was equal to the local inter-ommatidial angle of each lens (this proportion can be adjusted using the 'deltaPScale' variable). It is possible to perform a local smoothing operation on the data, whereby the optical axes and diameters of each lens are averaged with those of their neighbors. Smoothing may be useful if the visual parameters of an eye vary irregularly and can be adjusted using the 'smoothingFactor' variable.

To determine the fields of view (FOV) of each eye, we first calculated the intersection of each optical axis on a distant sphere. We then discretized the sphere into many equally spaced points and determined which of those points lay within a boundary enclosing the optical axis intersections. The points within the FOV were determined in this manner for each eye individually. The union of these two sets of points provided the total FOV, while the intersection indicated the portion of the FOV with binocular overlap. The borders around each region were also calculated for use in the later plotting steps; note that if multiple individual regions are present within a given field of view (such as in the binocular visual field, Fig. 2A), the border calculation may take a long time to compute. The visual sphere was also divided into individual regions for each lens. This was calculated either for the lenses of the left eye only (Fig. 2) or both eyes (Fig. 3) by calculating the borders of the voronoi cells (on the surface of the sphere) around the sphere intersection points of the lenses. Although the voronoi cells covered the entire sphere, those on the borders were limited to the extent of the previously calculated field of view.

Different methods were implemented to plot the data resulting from the previous analysis. The individual optical axes and fields of view were drawn onto a sphere surrounding a visualization of the head surface (Fig. S3A). The values of each calculated parameter ($\Delta\Phi$, D, P) were encoded using a color map, and displayed either as a world-based representation by coloring the voronoi cells of the left eye (Fig. 2A-C), or as a head-based representation by coloring the corneal lenses on the eye surface (Fig. 2A-C insets). While the voronoi cells were calculated on a sphere, we displayed them as 2D maps using an equirectangular projection, onto which either the binocular FOV or the right eye FOV could be displayed using the 'plotBinoLine' and the 'plotRightEyeLine' variables, respectively. It was also possible to draw contour lines of one parameter upon the map of another (for example contours of D on a map of $\Delta\Phi$ using the 'dispContourOnInterOImage' variable, Fig. S3B). Lenses viewing the binocular visual field could also be indicated with markers on the head centric representation (using the 'binoMarkerSize' variable). All plots could be saved automatically by setting the 'saveImages' flag.

To display color maps, the observed range of each calculated parameter was discretized into a number of equally spaced bins (set with 'numColBins' variable). By default, this discretization is performed for each insect, and different insect eyes had different ranges and receive different color mappings. To compare between multiple insects, 'AnalyseCorneaMain.m' should first be run for each insect with the 'saveData' flag set. This will save the calculated parameters for each insect analyzed and the 'PlotGroupHistograms.m' file (which requires similar variables to be set as in the main analysis file) was

used to produce overlaid histograms for the parameters, and to compute the mean, standard deviation, and range of each parameter for each insect. The latter file also determined the total ranges of each calculated parameter between all data sets and used them to compute the appropriate discretization for all insects. In the original file, the 'useGroupColBins' flag was then set, and re-running the main analysis file for each insect created plots with a common color mappings.

A simulation of an insect's vision of a user-supplied panoramic image (Fig. 3) or a checkered sphere (Fig. S3D) could also be computed (choose by setting the 'simUserIm' flag). When using the checkered sphere, the number of checks was set using the 'numChequers' variable, note that a higher number of checks results in a lower wavelength and higher spatial frequency, and that checks are mapped onto equirectangular image and do not represent equal angular areas on the world sphere (Fig. S3C). The simulation was performed using a direct rgb-to-grey scale conversion from the image provided as no knowledge of the spectral sensitivity of the simulated insects was available. The world coordinates were determined for each pixel of the image being used, and we simulated the insect's position at the center of the world sphere. For each lens, we averaged the intensity of all points that lay less than one inter-ommatidial angle from its corneal axis and weighted this average by a Gaussian kernel with full width at half maximum (FWHM) equal to the inter-ommatidial angle of each facet. We then shaded the facet's voronoi cell with the averaged grayscale value, and the simulation could either be performed for the left eye only or for both eyes by setting the 'simBothEyes' variable. The shaded cells were plotted on an equirectangular image in a similar manner to the color maps described above, and the border of the fields of view could also be displayed.

Upon acceptance of this manuscript: We will submit the Matlab files required to complete the analysis procedure described above as Supplementary Material.

Supplemental information

Supplemental Tables

Table S1: Summary of additional parameters related to each fungus gnat specimen. Field of view (FOV) is indicated as a percentage of the visual sphere viewed. Visual field extents are also provided as the minima and maxima angular limits of the total azimuthal range (at 0° elevation) and the total elevation range (at 0° azimuth), followed by the total angular extent in parenthesis (the visual field behind the head is indicated with values from -90° to -270° in the elevation range). The mean ± one standard deviation is provided for the lens diameter, inter-ommatidial angle, and eye parameter, followed by the measured minima and maxima values in parenthesis.

Species	*Neoplatyura modesta*	Orfeliini sp.	*Rutylapa* sp.
Habitat	Temperate forest	Tropical forest (Eocene)	Tropical forest
Collection location and year	Stenshuvud, Sweden (1977)	Lilla Beddinge, Sweden (1990)	West Usambaras Mountains, Tanzania (1990)
Preservation method	Dried	Endocast in amber	Alcohol
LE facet #	303	333	367
RE facet #	296	335	373
Head width (μm)	452	519	547
Left eye FOV (%)	48	55	46
Total FOV (%)	69	96	78
Binocular FOV (%)	27	17	15
Total azimuth range (°)	-138 – 138 (276)	-180 – 180 (360)	-128 – 135 (263)
Total elevation range (°)	-131 – 55 (186)	-228 – 44 (268)	-140 – 66 (208)
Lens diameter, *D* (μm)	19.2 ± 1.0 (14.7 – 23.4)	20.5 ± 1.3 (16.8 – 25.6)	20.1 ± 1.0 (17.7 – 25.1)
Inter-ommatidial angle, ΔΦ (°)	10.5 ± 4.5 (3.9 – 40.1)	11.3 ± 3.7 (6.0 – 28.5)	9.1 ± 2.8 (4.3 – 20.6)
Eye parameter, *P* (μm.rad)	3.6 ± 1.6 (1.3 – 14.1)	4.1 ± 1.4 (1.9 – 12.5)	3.2 ± 1.1 (1.4 – 9.0)

Table S2: The specific scan settings for the Zeiss XRM520 tomograph that were used for imaging. The 4x objective used for all samples.

Species	*Neoplatyura modesta*	Orfeliini sp.	*Rutylapa* sp.
Source voltage (kV)	80	80	50
Source power (W)	7	7	4
Exposure time (s)	2	10	10
Projections (#)	1,601	2,001	1,601
Source to rotation axis distance (mm)	15.0	21.0	14.0
Rotation axis to detector distance (mm)	86.3	120.9	80.0

Supplemental Figures

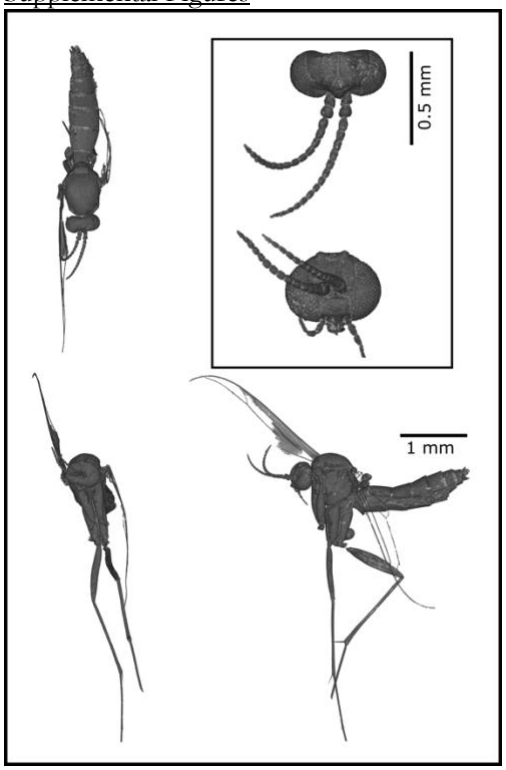

Figure S1: Habitus image created from the endocast of the female Eocene gnat specimen. Unfortunately, the degradation of the wings limited a full species identification of the sample, but the general morphological features place it in the tribe Orfeliini of the family Keroplatidae in the order Diptera.

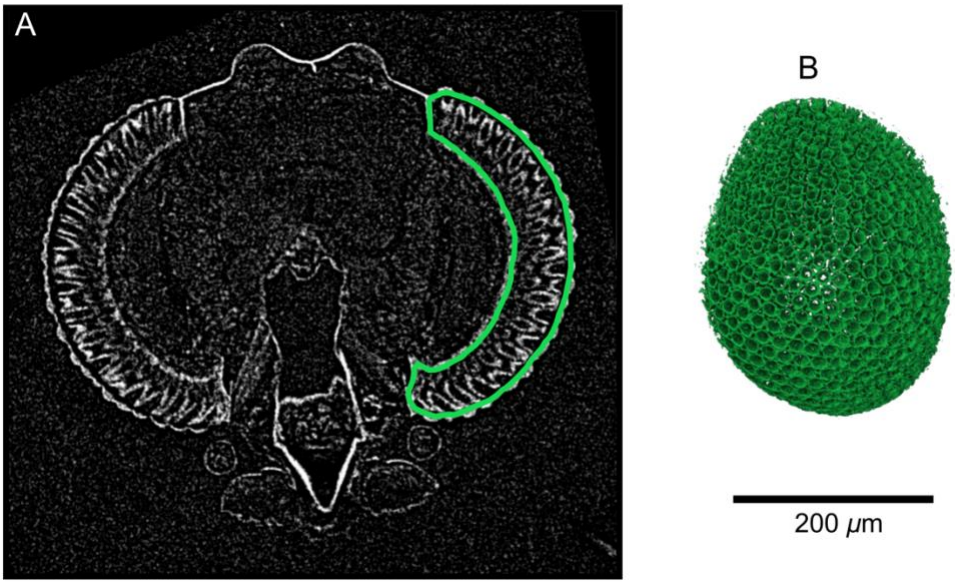

Figure S2: Internal structure of the alcohol-preserved *Rutylapa* sp. specimen. (**A**) A slice through the image volume shows that, in addition to the exterior cuticle, details within the retina of the eyes have high x-ray absorption. (B) We segmented the retinal volume of the left eye (enclosed by the green line in A), and used volume rendering to visualize the 3D retina. A conical x-ray absorbing structure is visible for each ommatidia, which may represent the secondary pigment cells surrounding the photoreceptors. The scale bar applies to both A and B.

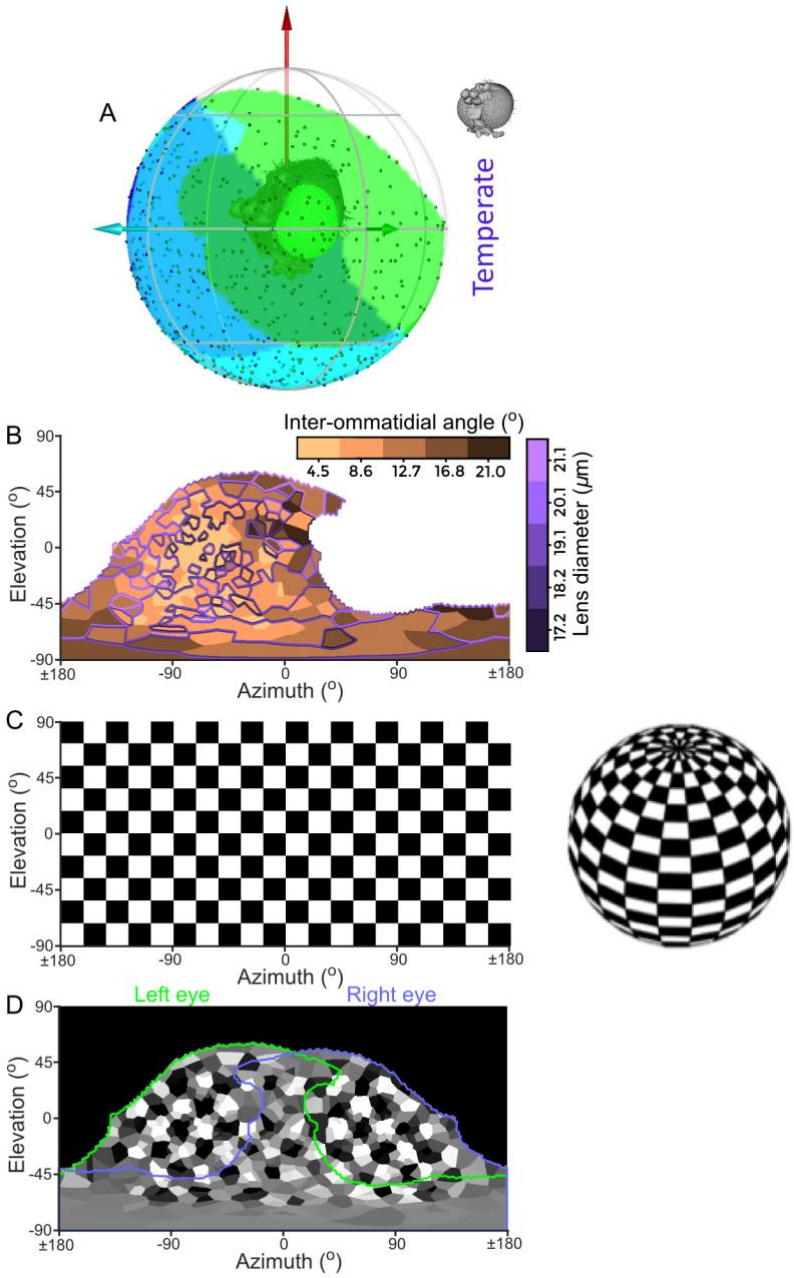

Figure S3: Examples of plotting options not used in the main text. (**A**) Head of a gnat plotted inside a sphere representing the world. Its left monocular, right monocular, and binocular visual fields are respectively represented by green, blue, and cyan shading on the sphere respectively. Points represent the intersection of the optical axes of individual lenses on the world sphere (as in Fig. 1Avii), and the green, cyan, and red arrows represent left lateral, frontal, and dorsal directions in the head-based reference frame. (**B**) Color map of the inter-ommatidial angle projection on the world, overlaid with colored contours representing the projected lens diameters. (**C**) Equirectangular projection (left) on a checkered sphere (right) with 36° period. (**D**) visual simulation of the gnat vision as if it was located inside the checkered sphere. The data used in this figure was from the temperate species *Neoplatyura modesta*.

References for main text and online methods

1 Land, M. F. & Nilsson, D.-E. *Animal eyes*. (Oxford University Press, 2012).
2 Land, M. F. Visual acuity in insects. *Annu. Rev. Entomol.* **42**, 147-177 (1997).
3 Cronin, T. W., Johnsen, S., Marshall, N. J. & Warrant, E. J. *Visual ecology*. (Princeton University Press, 2014).
4 Stavenga, D. G. in *Comparative Physiology and Evolution of Vision in Invertebrates: A: Invertebrate Photoreceptors* (ed H. Autrum) 357-439 (Springer Berlin Heidelberg, 1979).
5 Ribi, W. A., Engels, E. & Engels, W. Sex and caste specific eye structures in stingless bees and honey bees (Hymenoptera: Trigonidae, Apidae). *Entomol. Gen.*, 233-242 (1989).
6 Baird, E. & Taylor, G. X-ray micro computed-tomography. *Curr. Biol.* **27**, R289-R291 (2017).
7 Evenhuis, N. L. Catalog of the Keroplatidae of the world (Insecta: Diptera). *Bishop Mus. Bull. Entomol.* **13**, 1-178 (2006).
8 Kraemer, M. M. S. & Evenhuis, N. L. The first keroplatid (Diptera: Keroplatidae) species from the lower Eocene amber of Vastan, Gujarat, India. *Zootaxa* **1816**, 57-60 (2008).
9 von Tschirnhaus, M. & Hoffeins, C. Fossil flies in Baltic amber–insights in the diversity of Tertiary Acalyptratae (Diptera, Schizophora), with new morphological characters and a key based on 1,000 collected inclusions. *Denisia* **26**, 171-212 (2009).
10 Straw, A. D., Warrant, E. J. & O'Carroll, D. C. A 'bright zone' in male hoverfly (*Eristalis tenax*) eyes and associated faster motion detection and increased contrast sensitivity. *J. Exp. Biol.* **209**, 4339-4354 (2006).
11 Land, M. & Eckert, H. Maps of the acute zones of fly eyes. *J. Comp. Physiol. A* **156**, 525-538 (1985).
12 Heisenberg, M. & Wolf, R. *Vision in Drosophila: genetics of microbehavior*. Vol. 12 (Springer-Verlag, 1984).
13 Seidl, R. & Kaiser, W. Visual field size, binocular domain and the ommatidial array of the compound eyes in worker honey bees. *J. Comp. Physiol. A* **143**, 17-26 (1981).
14 Merry, J. W., Morehouse, N. I., Yturralde, K. & Rutowski, R. L. The eyes of a patrolling butterfly: Visual field and eye structure in the Orange Sulphur, *Colias eurytheme* (Lepidoptera, Pieridae). *J. Insect Physiol.* **52**, 240-248 (2006).
15 Beersma, D., Stavenga, D. & Kuiper, J. Retinal lattice, visual field and binocularities in flies. *J. Comp. Physiol.* **119**, 207-220 (1977).
16 Scales, J. A. & Butler, M. A. The relationship between microhabitat use, allometry and functional variation in the eyes of Hawaiian *Megalagrion* damselflies. *Funct. Ecol.* **30**, 356-368 (2016).
17 Mesler, M. R., Ackerman, J. D. & Lu, K. L. The effectiveness of fungus gnats as pollinators. *Am. J. Bot.*, 564-567 (1980).
18 Poinar, G. O. & Milki, R. *Lebanese amber*. (Oregon State University Press, 2001).
19 Streinzer, M. & Spaethe, J. Functional morphology of the visual system and mating strategies in bumblebees (Hymenoptera, Apidae, *Bombus*). *Zool. J. Linnean Soc.* **170**, 735-747 (2014).
20 Gonzalez-Bellido, P. T., Wardill, T. J. & Juusola, M. Compound eyes and retinal information processing in miniature dipteran species match their specific ecological demands. *Proc. Natl. Acad. Sci. U.S.A.* **108**, 4224-4229 (2011).
21 Tanaka, G., Parker, A. R., Siveter, D. J., Maeda, H. & Furutani, M. An exceptionally well-preserved Eocene dolichopodid fly eye: function and evolutionary significance. *Proc. R. Soc. Lond. B Biol. Sci.* **276**, 1015-1019 (2009).
22 Greco, M. K. *et al.* Description of an ancient social bee trapped in amber using diagnostic radioentomology. *Insectes Soc.* **58**, 487 (2011).
23 Lak, M. *et al.* Phase contrast X-ray synchrotron imaging: opening access to fossil inclusions in opaque amber. *Microsc. Microanal.* **14**, 251-259 (2008).
24 Suarez, A. V. & Tsutsui, N. D. The value of museum collections for research and society. *BioScience* **54**, 66-74 (2004).
25 Hölker, F., Wolter, C., Perkin, E. K. & Tockner, K. Light pollution as a biodiversity threat. *Trends Ecol. Evol.* **25**, 681-682 (2010).
26 Knop, E. *et al.* Artificial light at night as a new threat to pollination. *Nature* **548**, 206 (2017).
27 Collett, T. & Land, M. Visual control of flight behaviour in the hoverfly *Syritta pipiens* L. *J. Comp. Physiol.* **99**, 1-66 (1975).

28 Taylor, G. J. *et al.* The dual function of orchid bee ocelli as revealed by X-ray microtomography. *Curr. Biol.* **26**, 1319-1324 (2016).
29 Snyder, A. W. in *Comparative physiology and evolution of vision in invertebrates A: Invertebrate Photoreceptors* (ed H. Autrum) 225-313 (Springer Berlin Heidelberg, 1979).